Vision Research 188 (2021) 1–9

Contents lists available at ScienceDirect

Vision Research

journal homepage: www.elsevier.com/locate/visres

Spinning objects and partial occlusion: Smart neural responses to symmetry

Giulia Rampone [a,*], Alexis D.J. Makin [a], John Tyson-Carr [a], Marco Bertamini [a,b]

[a] Department of Psychology, University of Liverpool, Eleanor Rathbone Building, L697ZA Liverpool, UK
[b] Department of General Psychology, Via Venezia, 8 – 35131, University of Padova, Padova, Italy

ARTICLE INFO

Keywords:
Non-retinotopic sensory memory (nrSM)
Non-retinotopic reference-frame
Symmetry representation
ERP
Visual occlusion
Sustained Posterior Negativity

ABSTRACT

In humans, extrastriate visual areas are strongly activated by symmetry. However, perfect symmetry is rare in natural visual images. Recent findings showed that when parts of a symmetric shape are presented at different points in time the process relies on a perceptual memory buffer. Does this temporal integration need a retinotopic reference frame? For the first time we tested integration of parts both in the temporal and spatial domain, using a non-retinotopic frame of reference. In Experiment 1, an irregular polygonal shape (either symmetric or asymmetric) was partly occluded by a rectangle for 500 ms (T1). The rectangle moved to the opposite side to reveal the other half of the shape, whilst occluding the previously visible half (T2). The reference frame for the object was *static*: the two parts stimulated retinotopically corresponding receptive fields (revealed over time). A symmetry-specific ERP response from ~300 ms after T2 was observed. In Experiment 2 dynamic occlusion was combined with an additional step at T2: the new half-shape and occluder were rotated by 90°. Therefore, there was a moving frame of reference and the retinal correspondence between the two parts was disrupted. A weaker but significant symmetry-specific response was recorded. This result extends previous findings: global symmetry representation can be achieved in extrastriate areas non-retinotopically, through integration in both temporal and spatial domain.

1. Introduction

Visual perception relies on inputs from the retina, and shape information is integrated in the visual system to form coherent representations of the visual world. One source of information is the presence of regular (non-accidental) patterns in the environment that are associated with objects. The visual system is tuned to symmetry, both in humans (Barlow & Reeves, 1979; Carmody et al., 1977; Julész, 1981; Locher & Wagemans, 1993; Marković & Gvozdenovi, 2001; Wagemans et al., 1991; Wenderoth, 1994) and many other animals (Benard et al., 2006; Delius & Nowak, 1982; Grammer et al., 2003). In the Gestalt tradition, symmetry plays a fundamental role in perceptual organisation and figure-ground segmentation (Bertamini, 2010; Feldman, 2007; Machilsen et al., 2009; Mojica & Peterson, 2014; Treder & van der Helm, 2007). By definition, symmetry is characterized by rigid transformations (Jenkins, 1983; Wagemans et al., 1991, 1993). Models of symmetry perception involve computations that detect pairwise correlations across receptive fields (Dakin & Herbert, 1998; Dakin & Watt, 1994; Dakin & Hess, 1997; Garner, 1974; Jenkins, 1983; Osorio, 1996; van der Helm & Leeuwenberg, 1996; Wagemans et al., 1991, 1993; Zhu, 2014).

Neuroimaging and neurophysiology research provides important insights into the temporal and spatial dynamics of symmetry perception (Bertamini et al., 2018; Bertamini & Makin, 2014; Cattaneo, 2017). A symmetry-sensitive network has been found in the extrastriate regions – V3, V4 and Lateral Occipital Cortex, LOC (Chen et al., 2007; Keefe et al., 2018; Kohler et al., 2016; Sasaki et al., 2005; Tyler et al., 2005; Van Meel et al., 2019), with LOC playing a causal role in symmetry detection (Bona et al., 2014, 2015). Importantly, areas V1 and V2 do not show any symmetry-specific activation (Sasaki et al., 2005; Tyler et al., 2005; Van Meel et al., 2019). Electrophysiological (EEG) research has demonstrated an event-related potential (ERP) called the Sustained Posterior Negativity (SPN) (Höfel & Jacobsen, 2007; Makin et al., 2012, 2016; Martinovic et al., 2018; Norcia et al., 2002; Wright et al., 2018). The SPN is recorded over posterior electrodes and it is likely to be generated by the extrastriate symmetry network (Makin et al., 2012, 2016). This component is a relative measure (i.e. a difference wave), it has an onset latency of approx. 250–300 ms, and is sustained until stimulus offset (Bertamini et al., 2019). The SPN amplitude reflects the *perceptual goodness* of the stimulus: the more salient is the regularity the larger the amplitude (Makin et al., 2013, 2016, 2019; Palumbo et al., 2015).

* Corresponding author at: School of Psychology, Eleanor Rathbone Building, University of Liverpool, L7 7DL, UK.
E-mail address: giulia@liverpool.ac.uk (G. Rampone).

https://doi.org/10.1016/j.visres.2021.06.009
Received 8 March 2021; Received in revised form 4 June 2021; Accepted 19 June 2021
Available online 13 July 2021

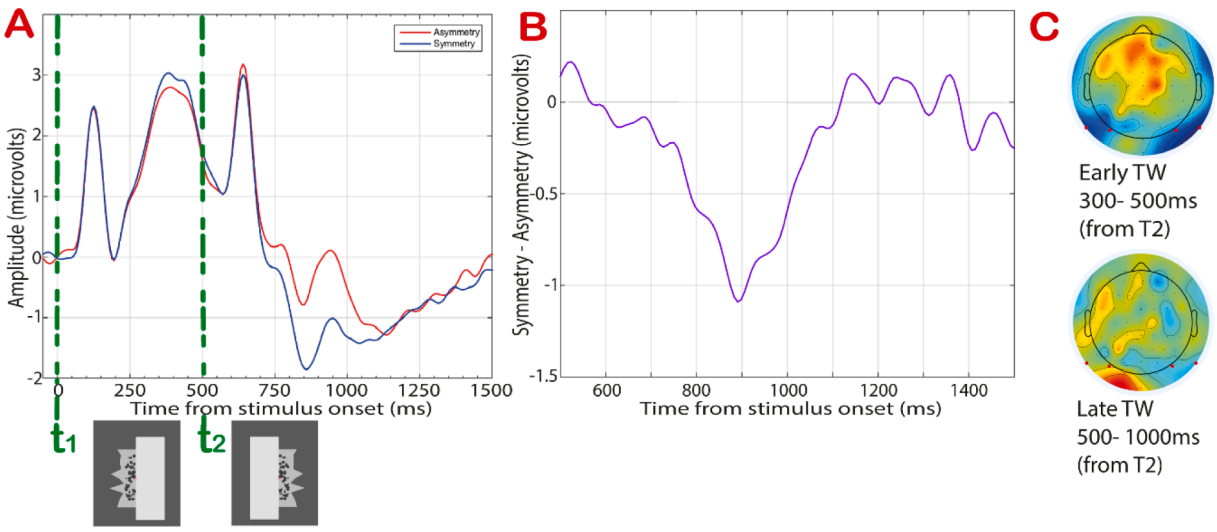

Fig. 1. Results taken from Rampone et al., (2019; Experiment 1). (A) Grand average ERPs averaged across electrodes P9 PO7 P10 PO8. From 0 ms (t1) to 500 ms the first half of a polygon shape was visible. At 500 ms (t2) the occluder moved and revealed the hidden half, whilst covering the previously visible part. After this, a symmetry – asymmetry ERP was observed after ~ 300 ms. The polygon shape could be either symmetric or asymmetric; the occluder could move either left → right or right → left. In the figure, an example of a symmetric shape with occluder moving right → left is reported. (B) Zoomed plot of the Grand average ERP shown as a difference wave (Symmetry – Asymmetry; solid purple) (C) Topographic difference maps (Symmetry – Asymmetry) from the time-window 300–500 ms and 500–1000 ms from T2. Red dots indicate electrodes analysed. (For interpretation of the references to colour in this figure legend, the reader is referred to the web version of this article.)

Most of the studies on the neural basis of symmetry perception use presentations with fully visible symmetry and long durations. However, in a dynamic and ever-changing natural environment, projection of objects onto the retina is constantly altered by both object and viewer's motion. One challenge for the visual system is that occlusions are ubiquitous in our environment and they remove significant shape information (Kourtzi & Kanwisher, 2001). To create a coherent representation, briefly-presented incoming information must be retained in a temporary perceptual buffer (*non-retinotopic Sensory Memory*, nrSM; Öğmen & Herzog, 2016) for a few hundred milliseconds, where it is integrated with new information (Ağaoğlu et al., 2012; Clarke et al., 2016; Öğmen & Herzog, 2016; Orlov & Zohary, 2018; Palmer et al., 2006; Scharnowski et al., 2007). This global *object-based* integration does not require a match in retinotopic coordinates (Öğmen & Herzog, 2016) and its output converges in extrastriate visual region and LOC (Kuai et al., 2017; Orlov & Zohary, 2018; Reichert et al., 2014; Yin et al., 2002).

Recently we demonstrated that the symmetry-network computes integration of parts during dynamic occlusion (Rampone et al., 2019). A complex polygon (either symmetric or asymmetric) was shown behind an occluder, so that only half was visible (always asymmetric; Fig. 1A). After a 500 ms interval, the occluder changed position and revealed a second half. No symmetry was ever in the image and it could only be detected by integrating the two parts (Fig. 1B). An SPN was generated, confirming a response within the symmetry-network (Fig. 1C-E). In Rampone et al. (2019) the object appeared static behind the occluder (dynamic occluder, static shape). In this case, elements of the shape remained within a static *reference frame*, which guides the attribution of stimulus features according to group identity (Lauffs et al., 2019). One could argue that the preserved retinotopic correspondences within the static *reference frame* allowed symmetry perception. On the contrary, if shapes were displaced (e.g., moving to a different location at t2) the *reference frame* would change; integration should be thus achieved across both the temporal and spatial dimension. Such condition tests whether the visual system can extract global symmetry non-retinotopically.

We tested integration of symmetry in dynamic occlusion with a *static* (Experiment 1) and a *moving frame of reference* (Experiment 2). The symmetry axis was always set at 45° (Fig. 2) and the occluder position changed. When the shape remained static, the parts stimulated retinotopically matching locations (only temporal integration required). In Experiment 2, the *reference frame* rotated by 90° at t2 (at same time as the occluder moved; see Fig. 4), so the parts stimulated unrelated retinotopic locations (spatiotemporal integration required). The results demonstrate the flexibility of the symmetry-sensitive network, which activity is not subordinate to rigid early computations but can reflect global interactions of spatial correlations.

2. Experiment 1

Here we tested *temporal integration* of two asymmetric halves of a polygon shape into a global representation of its symmetry. A rectangle bar acted as a dynamic occluder covering one half of the shape for 500 ms, and then the other half for 1000 ms. No symmetric configuration was visible on any given frame (more precisely, what was symmetrical, such as the occluder, was the same in all frames). Participants decided whether the perceived static whole was symmetric or asymmetric.

2.1. Method

2.1.1. Participants

Twenty-eight participants took part in the experiment (mean age = 32.2, SD = 15, range = 54; 8 males; 5 left-handed). Sample size was selected a priori for consistency with Rampone et al. (2019). Participants had normal or corrected-to-normal vision. Some received course credit upon completion of the study. The study was approved by the University of Liverpool Ethics Committee (reference: 2122). The experiment was conducted in accordance with the Declaration of Helsinki (although the study was not pre-registered, which is required by point 35 of the 2008 revision).

2.1.2. Apparatus

EEG activity was recorded using a BioSemi Active-Two amplifier in an electrically shielded and darkened room. EEG data were sampled continuously at 512 Hz from 64-scalp electrodes embedded in an elasticised cap arranged according to the standard international 10–20

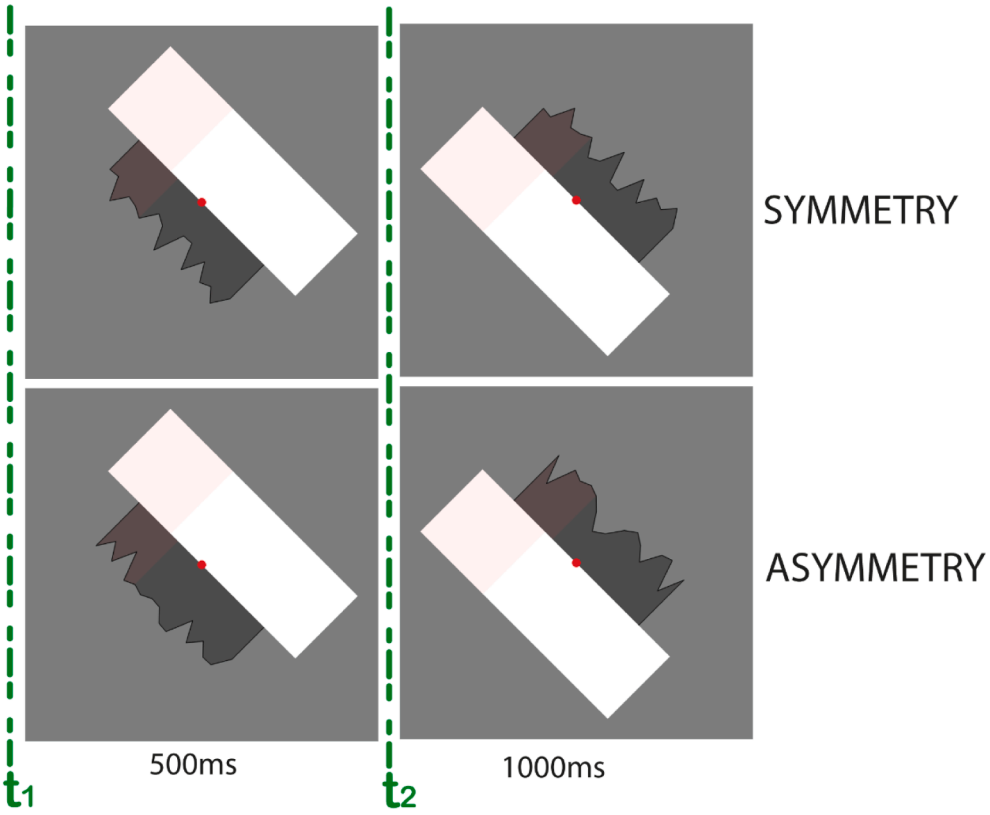

Fig. 2. Example of the stimuli and experimental procedure. In the top row the shapes (dark-grey polygons) match to form bilateral symmetry; the shapes on the bottom row do not match. No single frame of the display ever contained the full symmetric shape. The tops of occluder and polygon were red to help participants in keeping track of the reference frame. The procedure was same as Rampone et al. (2019; described in Fig. 1A). All stimuli were generated afresh, and a new stimulus was presented on each trial. (For interpretation of the references to colour in this figure legend, the reader is referred to the web version of this article.)

system. Electrode offset was maintained within the −25 + 25 μV range for all electrodes. To detect blinks and eye movements, vertical bipolar electrodes (VEOG) were positioned above and below the right eye. Horizontal bipolar electrodes (HEOG) were positioned on the outer canthi of both eyes. Stimuli and experiment were programmed using PsychoPy software (Peirce, 2007) and presented on a CRT monitor (60 Hz; resolution: 1280 × 1024). Participants were positioned 140 cm from the monitor with their head stabilised in a chin rest.

2.1.3. Stimuli

Stimuli consisted of complex polygons (bottom part grey (RGB [−0.4, −0.4, −0.4], CIEXYZ [0.29, 0.30, 0.33][1], luminance 15.5 cd/m2); top part red (RGB [−0.3, −0.4, −0.4], CIEXYZ [0.31, 0.31, 0.33], luminance 15.8 cd/m2)). The occluder was a white bar (RGB [0.8, 0.8, 0.8], CIEXYZ [0.86, 0.90, 0.98], luminance 178 cd/m2), with red top (RGB [1, 0.9, 0.9], CIEXYZ [0.92, 0.96, 1.04] luminance 166 cd/m^2). The stimuli were presented on a grey background (RGB [-0.3, -0.3, -0.3], CIEXYZ [0.33, 0.35, 0.38], luminance 42.6 cd/m^2) (Peirce, 2007). All shapes were generated afresh on each trial. No participant ever saw the same pattern twice.

Polygons were generated by creating one half first, with a random-walk algorithm (16 inward and outward turns). The second half was either generated independently (asymmetry condition) or it was mirrored (symmetry condition). Each turn was spaced approx. 0.5° longitudinally and had a maximum and minimum transverse displacement of approx. ± 0.9°. Top and bottom vertices were connected with straight lines to form a closed polygon (height approx. 7.7°). The red-coloured part measured approx. 2° (4 turns). The occluder was a rectangle (approx. 5.6 X 11.3°). One side of the occluder was aligned with the polygon to give the impression of occlusion. The configuration had an inclination of 45° from the midline.

2.1.4. Procedure

Prior to the start of the experiment, participants completed a practice block to give them the opportunity to familiarise with the task. In the practice block a response feedback (i.e. sound for incorrect responses) was provided; this was not present in the experimental block. A practice block consisted of 16 trials; participants were given the possibility to repeat as many blocks as they wished until confidence with the task was reached. Participants were required to maintain fixation during the whole trial and refrain from blinking when stimuli were displayed. Breaks were provided during the experiment to allow participants to rest.

The sequence of events is described in Fig. 2. A short interval (500 ms) with only the fixation dot on screen, was followed by the baseline period (1500 ms) in which the occluder was shown (no polygon). The occluder could be either at the left or right side of the central fixation (counterbalanced across trials). After baseline, the stimulus appeared (t1). Only half of the stimulus was visible on the side not occupied by the occluder. At this point, participants could not predict whether the stimulus was symmetry or asymmetry. The first half remained visible for 500 ms (t_1). The occluder was displaced and the second half of the

[1] Note that due to COVID19 situation we could not access the labs for measuring CIE coordinates precisely. The ones provided are estimations, which assume sRGB space for the conversion and a D65 white point.

pattern revealed. This remained on the screen for 1000 ms (t_2)[2]. Stimulus recognition was supposed to happen at this time-window. A response message then appeared superimposed to the stimulus (i.e., "Symmetry Asymmetry" or "Asymmetry Symmetry", counterbalanced across trials). Participants entered a response, by pressing either the 'A' or 'L' key of the computer keyboard with their left or right index fingers. They were explicitly informed that responses needed to be as accurate as possible, whilst response speed was not measured. This minimized motor responses artifacts during the stimulus presentation period. The experiment consisted of a total of 336 trials (84 X 4 sub-conditions).

2.1.5. Data analysis

EEG data was processed using the EEGLAB v2019.1 toolbox in MATLAB (Delorme & Makeig, 2004) and the same criteria as in Rampone et al., (2019). Data was imported using Cz as reference and then re-referenced to a scalp average (using *pop_reref*). Filtering operations used *pop_eegfiltnew*, high-pass filter 0.1 Hz and low-pass filter 25 Hz. Data were then down-sampled to 128 Hz (*pop_ resample*), segmented into −1 to 2 s epochs (*pop_epoch*) and set to baseline (-200 ms; *pop_rmbase*). Independent Components Analysis (ICA) was used (*pop_runica*) to remove oculomotor and other gross artefacts. ICA components were removed manually through visual inspection. On average 9.7 (SD = 3.4) of 64 independent components were removed from each participant (min = 4, max = 17). If bad channels were identified, *pop_interp()* was used for spherical interpolation. Moreover, trials where participants entered incorrect response were marked in the dataset for exclusion. Finally, trials where amplitude exceeded +/- 100 μV at any electrode were excluded (*pop_eegthresh*). In some cases, epoch rejection was performed with additional visual inspection in EEGLAB. Data were then re-referenced to scalp average and set to baseline. Individual averages for each condition were generated for final Grand-average ERP analysis. Criteria for inclusion were behavioural performance and EEG data quality. All participants made > 70% of correct responses, so none was excluded on this basis. Because of the large number of trials, we could include datasets with up to 50% of total trials rejection (corresponding to > 80 trials per condition). No participant was excluded in Experiment 1. After data cleaning, the average number of trials included was 116.75 (SD = 25) for Symmetry and 115.07 (SD = 24) for Asymmetry.

For the ERP analysis, we used a cluster of posterior electrodes (left hemisphere: P9, PO7; right hemisphere: P10, PO8; same as Rampone et al., 2019). PO7/PO8 best represent the topographical distribution of the SPN (Martinovic et al., 2018; Wright et al., 2018; Makin et al., 2016, 2012). The amplitude of the Symmetry – Asymmetry difference was recorded starting from 300 ms after onset of the second half (t_2 = 500 ms). We split the SPN in two timewindows: eSPN, 800–1000 ms (300–500 ms from t_2); lSPN, 1000–1500 ms timewindow (500–1000 ms from t_2). This choice was made a priori based on the observations from Rampone et al. (2019) and other works (Makin et al., 2016; Wright et al., 2017). These authors have suggested that the earlier SPN peaks ~ 400 ms.

The ERPs data were normally distributed (Shapiro-Wilk tests p > .05). These were analysed with repeated measure ANOVA and *t*-test; the Greenhouse-Geisser test correction factor was used when the assumption of sphericity was violated (Mauchly's test, p > .05). Behavioural accuracy data were not normally distributed (Shapiro-Wilk test p < .05). For Asymmetry and Symmetry Proportion incorrect responses were: Asymmetry median 12.5%; Symmetry median 8.6%. All materials for re-running the experiments and re-analyzing the results are available on Open Science Framework (https://osf.io/c7bdg/). The data from this study also appear in the Complete Liverpool SPN Catalogue (Project 28; https://osf.io/2sncj/) along with other data from the University of Liverpool. The study was not preregistered, but all hypotheses and analyses were planned priori (based on analyses and results of Rampone et al., 2019).

[2] The terminology used in the description reflects the percept of (dynamic) occlusion. There is no actual physical occlusion in these stimuli. Hence, events within a trial may be described as follows. An irregular polygon was shown next to a rectangle. In the second interval, a rectangle was presented at the location of the first polygon, and a second irregular polygon was shown where the rectangle was before. In half of the trials the two polygons were one the reflection of the other, and in the other half the two polygons were unrelated. We assume, in line with literature, that objects may exist at the amodal level (Michotte et al., 1964; Thielen et al., 2019). Similarly, when we refer to movement of the occluder, the motion is implied by a change of location.

2.2. Results

Fig. 3A shows the Grand Average ERP (electrodes P9 PO7 – left; P10 PO8 - right) for symmetry and asymmetry. Onset of the first polygon is marked as t1. In the t1-t2 timeframe (500 ms) no difference between the two waves is present; here stimuli are all asymmetric. After approx. 300 ms from t2 the SPN component emerges. This response remained sustained until the end of the epoch.

We calculated the SPN as a difference wave between symmetry and asymmetry (Fig. 3B). A 2X2 ANOVA was conducted to assess differences in SPN across timewindows and hemispheres. A main effect of timewindow was obtained ($F_{(1,27)} = 4.77$, $p = .04$, $\eta^2_p = 0.01$) and no effect of hemisphere or interaction ($F < 1$, $p > 0.3$). Amplitude in the eSPN (300–500 ms from t_2) measured −0.83 μV (SD = 0.81) and was significantly below zero ($t_{(27)} = -5.40$, $p < .001$, $dz = -1.02$). Amplitude in the lSPN (500–1000 ms from t_2) was −0.50 μV (SD = 1.16) and was significantly below zero ($t_{(27)} = -2.28$p = .01, dz = -0.43). In the earlier timewindow 25/28 (=0.89) participants showed a lower amplitude in the symmetry condition; this was reduced to 18/28 (=0.64) in the late SPN. Fig. 3B shows the difference wave (solid black) along with 95% confidence intervals (C.Is; thick dashed lines) and individual-subject responses (thin dashed lines). Individual amplitude distributions, separately for each hemisphere and timewindow, are plotted in Fig. 3D. In Fig. 3C the difference amplitude is shown in topographic maps.

2.3. Discussion of Experiment 1

Experiment 1 replicated the results of Rampone et al (2019). Two parts can be temporally integrated within a *fixed retinotopic reference frame* to form a symmetry percept. There was an SPN, and its amplitude was larger in the earlier part of the component. This strengthens the conclusion that the extrastriate symmetry-network responds to symmetry as a property of an integrated whole.

Can the extrastriate network integrate the matching parts even when retinotopic correspondence is disrupted? This question was addressed in Experiment 2, where a *moving reference frame* was used.

3. Experiment 2

Stimuli and sequence of events were same as in Experiment 1, with an additional step at t2: both occluder and shape rotated by 90°. Therefore, not only the occluder moved from one side to the other, but the whole stimulus' *reference frame* was rotated. Because of this rotation, the two parts did not match in the retinal image (Fig. 4). Detection of spatial correspondence between parts must happen at object-level (non-retinotopic).

3.1. Method

Thirty participants took part in the Experiment 2 (mean age = 29.6, SD = 12.3, range = 38; 6 males; 4 left-handed). Data from two participants were rejected because of problems during EEG recording (i.e., trigger information missing in the data) and high level of noise (trials rejection > 50% of total trials), leading to a total of twenty-eight participants. Stimuli and apparatus where same as Experiment 1. The

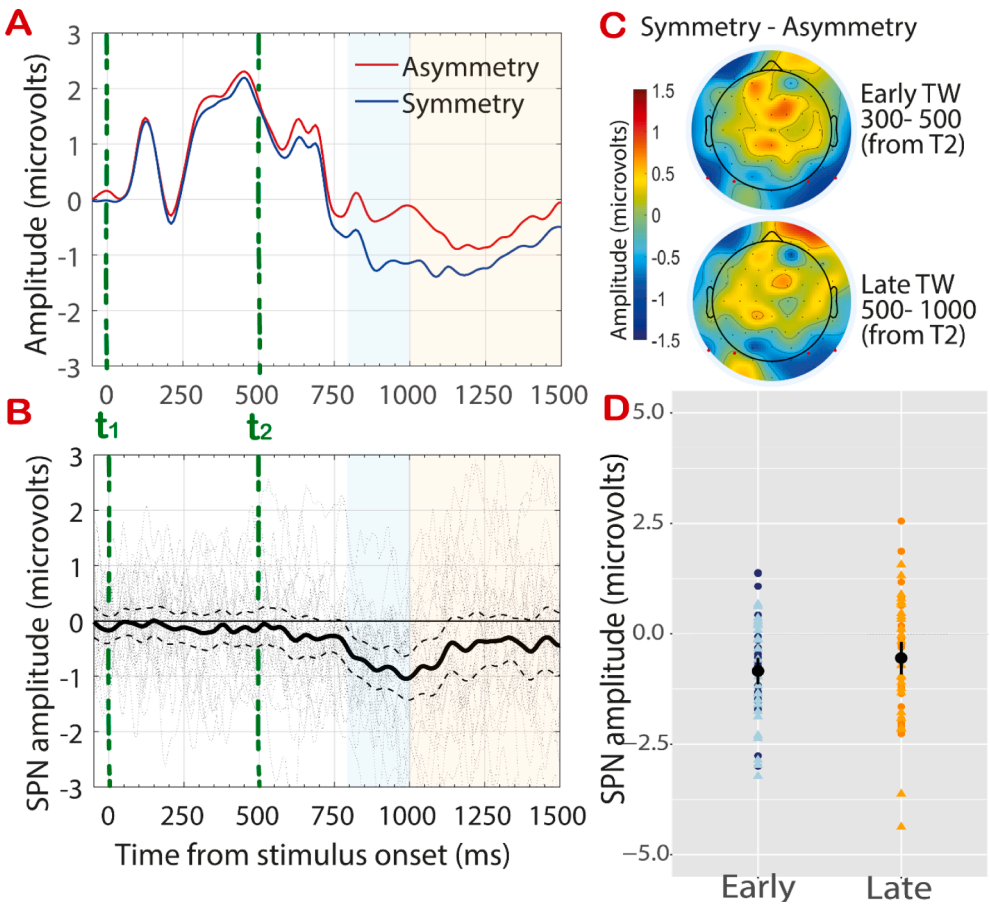

Fig. 3. (A) Grand average ERPs averaged across electrodes P9 PO7 P10 PO8. A SPN is observed after ~ 300 ms from T2. (B) The SPN (difference wave: Symmetry – Asymmetry; solid black) is shown along with 95% confidence intervals (C.I; thick dashed black lines) and individual-subject responses (thin dashed black lines). The blue and orange regions indicate the time-windows used for the analysis. (C) Topographic difference maps (Symmetry – Asymmetry) from the time-window 300–500 ms and 500–1000 ms from T2. Red dots indicate electrodes analysed. (D) Stripcharts (i.e. one- dimensional scatter-dot plots) showing distributions of difference amplitudes for the two-time windows; dark-coloured dots represent responses at the left hemisphere; light-coloured triangles represent responses at right hemisphere. Mean difference amplitude is superimposed (black dot), and error bars indicate 95% C.I. (For interpretation of the references to colour in this figure legend, the reader is referred to the web version of this article.)

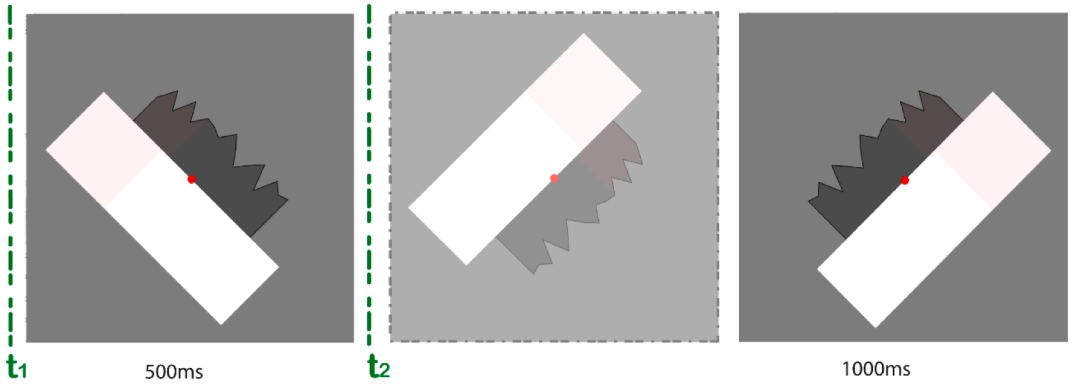

Fig. 4. Example of stimuli and procedure in Experiment 2. The sequence of events was the same as in Experiment 1, with an additional step at t2: both occluder and shape rotated by 90° and at the same time the occluder translated. The lighter central image is displayed for illustration purposes but was not present in the experiment. Only the first half of the practice included a brief presentation (6 ms) of this stage to help familiarisation with the rotating frame of reference.

critical difference is that at t2 there were two changes: the occluder was presented at the opposite side of fixation (as in Experiment 1) and the whole stimulus (occluder + polygon) was presented at an orientation of 45° from vertical. This gave the impression that, while the occluder changed position over the object, both stimuli rotated by 90° (see Fig. 4). Note that, because of the rotation, the second half was superimposed to the same retinal location as the previous half. Participants familiarised with the task during two practice blocks (16 trials each). The first block included the presentation of a vertical stimulus, between initial and final orientations (-45° > 0 > 45°). This facilitated the perception of rotation. The second block of the practice was identical to the experiment, with two presentations: occluder and polygon (t1-t2); occluder and polygon rotated (t2-end of epoch).

After the EEG data processing, an average of 123.2 (SD = 16.1; symmetry) and 123.7 (SD = 18.4; asymmetry) trials were considered for analysis (average independent components removed after ICA = 8.9, SD = 2.6). ERP data were normally distributed (SW $p > .05$), whilst behavioural data were not. Behavioural performance was > 75% for all participants. Proportion incorrect responses was below chance for both symmetry (median = 9.5) and asymmetry (median = 14.3).

3.2. Results

Fig. 5A shows the Grand Average ERPs. A symmetry response was

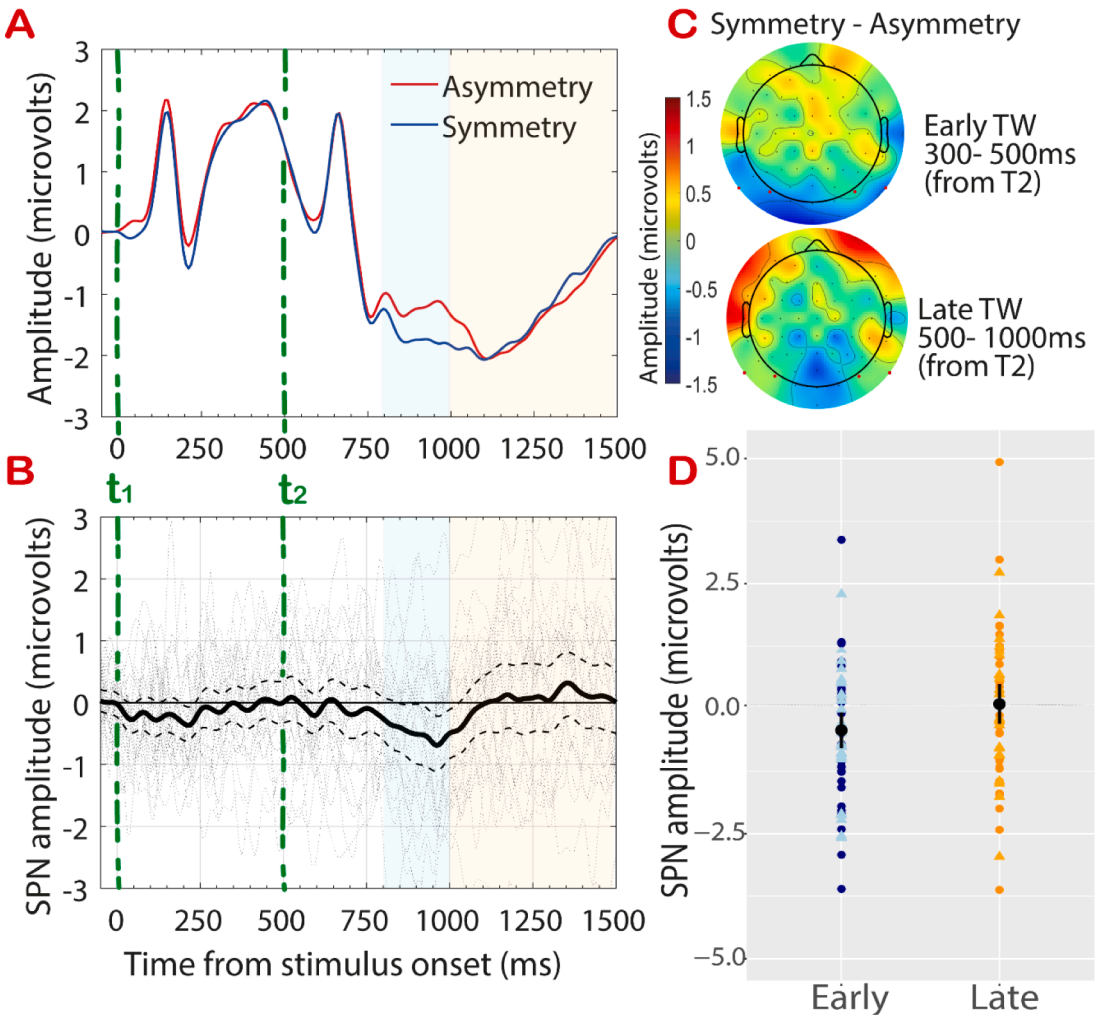

Fig. 5. *Experiment 2 Results* (A) Grand average ERP waves averaged across electrodes P9 PO7 P10 PO8. (B) Grand average ERP shown as a difference wave (Symmetry – Asymmetry; solid black) with 95% C.I (thick dashed) and individual responses (thin dashed) (C) Topographic difference maps (Symmetry – Asymmetry) from 300 to 500 ms and 500–1000 ms from t2 (D) Stripcharts showing distributions of individual amplitudes at the two-time windows analysed; dark dots and light triangles represent left and right hemisphere, respectively. Mean difference amplitude is superimposed (black dot), and error bars indicate 95% C.I.

triggered approx. 300 ms after t2, although this was smaller in amplitude and shorter in latency compared to Exp 1. The 2 (timewindow) X 2 (hemisphere) ANOVA was conducted on the difference wave. A main effect of timewindow was obtained ($F_{(1,27)} = 12.25$, $p = .002$, $\eta^2 = 0.03$); no effect of hemisphere or interaction ($F < 0.3$, $p > 0.5$). Amplitude in the eSPN (300–500 ms from t_2) measured −0.49 μV (SD = 1.08) and was significantly below zero ($t_{(27)} = -2.43$, $p = .02$, $dz = -0.46$). Amplitude in the lSPN (500–1000 ms from t_2) was 0.02 μV (SD = 1.20; $t_{(27)} = -0.10$, $p = .92$, $dz = -0.02$). In the earlier timewindow 17/28 (=0.6) participants showed lower amplitude in the symmetry condition; this was reduced to 14/28 (=0.5) in the later part of the SPN. Fig. 5B shows the difference wave, with 95% confidence intervals and individual-subject responses. This is plotted in Fig. 5D as stripcharts of the individual amplitude distributions. Fig. 5C shows topographic maps of the difference amplitude.

3.3. Discussion Experiment 2

In this experiment a *rotating reference frame* meant that the two shape-halves appeared at different overlapping locations. Participants performed the task above chance (>80% proportion correct) and a response to symmetry was elicited from the extrastriate network (SPN), although this was smaller in amplitude and not sustained. This result shows that a global representation of symmetry can be achieved through integration of parts both in the temporal and spatial domain.

4. General discussion

A symmetry-sensitive network is in extrastriate areas, regions that are sensitive to shape and objectness. Most research has focused on responses to symmetry in the visual image, with some exceptions looking at perspective normalisation (Makin et al., 2015; Keefe et al., 2018) and dynamic occlusion (Rampone et al., 2019). The latter study showed that when (irregular) parts of a symmetric shape are shown at different points in time, the visual system can retain information and integrate it with newer information. The output of this integration was evidenced by an ERP component known as Sustained Posterior Negativity (SPN) (Makin et al., 2016; Rampone & Makin, 2020). In Rampone et al (2019) stimuli were presented within a *static reference frame*. Such condition left open the question of whether this temporal integration can be achieved at more global level. The current study challenged the symmetry-sensitive network by adding a *rotating reference frame* (occluder + polygon). A global representation of symmetry could be achieved only through spatiotemporal integration in a non-retinotopic reference frame.

Experiment 1 used a *static reference frame*. Participants saw a rectangle covering half of a polygon shape (t1) and then moving to reveal the other part (t2). The two parts could produce either a symmetric or

asymmetric object. We found an SPN-like response starting approx. 300 ms from t2. Experiment 2 used a *moving reference frame*: both shape and occluder rotated by 90° at t2 (in addition to the displacement of the occluder). This disrupted the correspondence in retinotopic coordinates between the two parts. Moreover, the rotation caused spatial overlap: the two halves stimulated part of the same receptive fields. A symmetry-response was confirmed after t2, albeit with smaller amplitude and shorter latency than in Experiment 1. This demonstrates the two halves were integrated, and a symmetry representation was elicited in the extrastriate network.

This finding is consistent with behavioural literature showing that object recognition in dynamic occlusion is achieved *non-retinotopically*. For example, in anorthoscopic vision (i.e. a stimulus moving behind a narrow slit) information about the moving object overlaps temporally on a narrow retinotopic locus. Stimulus fragments are stored in a sensory buffer (*non-retinotopic Sensory Memory*, *nrSM*; Öğmen & Herzog, 2016) so that the information is not erased by new inputs to the same receptive fields. Motion mechanisms provide the reference frame used to compute non-retinotopically features of moving targets (Aydın et al., 2008; Clarke et al., 2016; Noory et al., 2015; Ogmen et al., 2010). In our Experiment 2, the second half was superimposed to the location previously occupied by the first half. This means the visual system could not use information from a retinotopic map. The output of the symmetry computation was indexed by a SPN-like response over extrastriate areas, in line with literature showing spatiotemporal integration at the level of LOC (Kuai et al., 2017; Orlov & Zohary, 2018; Reichert et al., 2014; Yin et al., 2002).

It is important to consider possible confounds in the results observed: the SPN-like component in t2 may not reflect symmetry-related activity. The task employed in this study might rather involve *change detection* processes. For example, the information in t1 might be retained in SM, flipped to mirror reversal and then matched to the information in t2. This process would probably be more computationally demanding than integrating corresponding parts according to the motion of stimuli (Öğmen & Herzog, 2016). However, it is a possibility we cannot exclude. Change detection, between two sequentially presented stimuli, yields centro-parietal positivity at approx. 300 ms from onset of the (changed) stimulus (falling into the class of P300 potentials; Koivisto & Revonsuo, 2003; Niedeggen et al., 2001). In 2-AFC tasks, participants may tend to perceive the most salient stimulus as the target (i.e. symmetry, in this case) and the other condition as target absent (i.e. asymmetry). Makin et al., (2012) addressed this question and observed that the SPN was generated irrespective of whether symmetry or asymmetry were the target. We would thus exclude that our result reflected a *target-change* (or *target-same*) detection. Moreover, the latency and topography of the component reported here corresponded to our predictions and was localised in a cluster of electrodes around PO7, PO8 (which consistently show largest symmetry-related activity, e.g. Bertamini et al., 2018; Makin et al., 2012, 2016). Finally, in Rampone et al (2019)'s Experiment 4 and 5 the integration of symmetric parts was compromised by either lack of sense-of-*objectness* or task demands, respectively. Even when symmetry was task relevant (Experiment 4), no symmetry – asymmetry ERP difference was measured. This would be unexpected if the component reflected a *target-change* detection. Orientation-normalisation processes might also affect ERP responses at parietal level (Heil, 2002; Quan et al., 2017). However, it is unlikely that the component observed here reflected a rotation-related negativity, because all stimuli (both symmetric and asymmetric) underwent the same rotational transformations.

The SPN had shorter latency in Experiment 2 than in Experiment 1 (ending approx. 500 ms from t2). Previous studies have shown that the early part of the SPN component (peaking at 400 ms from onset) more reliably indexes the perceptual representation of stimulus regularity (Makin et al., 2016; Rampone et al., 2019; Wright, Makin, & Bertamini, 2017). The second part of the component (from 500 ms to end of epoch) is more variable and possibly subject to re-entrant processes or deployment of spatial attention.

The increasing computational demands of Experiment 2 may explain reduced amplitude and shorter latency of the SPN. We know that the SPN amplitude is highly sensitive to the salience of the regularity (Makin et al., 2016, 2019; Palumbo et al., 2015). Moreover, we have learned that effortful processes (e.g. temporal integration, Rampone et al., 2019; perspective normalisation, Keefe et al., 2018; Makin et al., 2015) draw on neural resources and do not happen automatically (see also Supplementary Material showing no response to symmetry in trials where incorrect responses were entered). It is thus not surprising that such a challenging task affects the ERP response to symmetry. Alternatively, lower amplitude in Experiment 2 may be due to participants not sensing the two halves as belonging to the same (rotated) object. Rampone et al (2019) showed that a sense of objectness is important for the integration-SPN to be generated. Possibly, a stimulus designed to convey a stronger sense of motion/rotation may have elicited a stronger symmetry response. However, note that the practice block in Experiment 2 included an additional step at t2 (see Fig. 4), which was specifically designed to train participant and facilitate the perception of a 90° rotation.

Our findings are in line with behavioural studies demonstrating global processes for symmetry representation (Niimi et al., 2005, 2008; Sharman & Gheorghiu, 2017, 2018, 2019; Tyler, 1995). On the contrary, classic models of symmetry perception emphasise early responses to pairwise correlations in the image (Poirier & Wilson, 2010; Dakin & Herbert, 1998; Dakin & Watt, 1994; Dakin & Hess, 1997; Osorio, 1996; Jenkins, 1983; Wagemans et al., 1991; Wagemans et al., 1993; van der Helm & Leeuwenberg, 1996; Garner, 1974; Zhu, 2014). It is necessary for models to be updated so that they can rely not only on information present at the retinotopic level. In turn, these changes will provide greater ecological validity.

Our results highlight the flexibility of mechanisms for symmetry perception. We conclude that extrastriate representation of symmetry is achieved from integration of temporally and spatially fragmented information.

CRediT authorship contribution statement

Giulia Rampone: Conceptualization, Methodology, Investigation, Formal analysis, Writing - original draft, Writing - review & editing. **Alexis D.J. Makin:** Conceptualization, Writing - review & editing, Funding acquisition. **John Tyson-Carr:** Formal analysis, Writing - review & editing. **Marco Bertamini:** Conceptualization, Methodology, Writing - review & editing.

Acknowledgments

This project was part funded by an ESRC grant (ES/S014691/1) awarded to Alexis Makin. We would like to thank the project student Catherine Rigby for helping with data collection.

Appendix A. Supplementary data

Supplementary data to this article can be found online at https://doi.org/10.1016/j.visres.2021.06.009.

References

Ağaoğlu, M. N., Herzog, M. H., & Öğmen, H. (2012). Non-retinotopic feature processing in the absence of retinotopic spatial layout and the construction of perceptual space from motion. *Vision Research, 71*, 10–17. https://doi.org/10.1016/j.visres.2012.08.009.

Aydın, M., Herzog, M. H., & Öğmen, H. (2008). Perceived speed differences explain apparent compression in slit viewing. *Vision Research, 48*(15), 1603–1612. https://doi.org/10.1016/j.visres.2008.04.020.

Barlow, H. B., & Reeves, B. C. (1979). The versatility and absolute efficiency of detecting mirror symmetry in random dot displays. *Vision Research, 19*(7), 783–793. https://doi.org/10.1016/0042-6989(79)90154-8.

Benard, J., Stach, S., & Giurfa, M. (2006). Categorization of visual stimuli in the honeybee Apis mellifera. *Animal Cognition, 9*(4), 257–270. https://doi.org/10.1007/s10071-006-0032-9.

Bertamini, M. (2010). Sensitivity to reflection and translation is modulated by objectness. *Perception, 39*(1), 27–40. https://doi.org/10.1068/p6393.

Bertamini, M., & Makin, A. D. J. (2014). Brain Activity in Response to Visual Symmetry. *Symmetry, 6*(4), 975–996. https://doi.org/10.3390/sym6040975.

Bertamini, M., Rampone, G., Oulton, J., Tatlidil, K. S., Makin, A. D. J. D. J., Tatlidil, S., & Makin, A. D. J. D. J. (2019). Sustained response to symmetry in extrastriate areas after stimulus offset: An EEG study. *Scientific Reports, 9*(1). https://doi.org/10.1038/s41598-019-40580-z.

Bertamini, M., Silvanto, J., Norcia, A. M., Makin, A. D. J., & Wagemans, J. (2018). The neural basis of visual symmetry and its role in mid- and high-level visual processing. *Annals of the New York Academy of Sciences, 1426*, 1–16. https://doi.org/10.1111/nyas.13667.

Bona, S., Cattaneo, Z., & Silvanto, J. (2015). The Causal Role of the Occipital Face Area (OFA) and Lateral Occipital (LO) Cortex in Symmetry Perception. *Journal of Neuroscience, 35*(2), 731–738. https://doi.org/10.1523/JNEUROSCI.3733-14.2015.

Bona, S., Herbert, A., Toneatto, C., Silvanto, J., & Cattaneo, Z. (2014). The causal role of the lateral occipital complex in visual mirror symmetry detection and grouping: An fMRI-guided TMS study. *Cortex, 51*(1), 46–55. https://doi.org/10.1016/j.cortex.2013.11.004.

Carmody, D. P., Nodine, C. F., & Locher, P. J. (1977). Global detection of symmetry. *Perceptual and Motor Skills, 45*(3 Pt 2), 1267–1273. https://doi.org/10.2466/pms.1977.45.3f.1267.

Cattaneo, Z. (2017). The neural basis of mirror symmetry detection: A review. *Journal of Cognitive Psychology, 29*(3), 259–268. https://doi.org/10.1080/20445911.2016.1271804.

Chen, C. C., Kao, K. L. C., & Tyler, C. W. (2007). Face configuration processing in the human brain: The role of symmetry. *Cerebral Cortex, 17*(6), 1423–1432. https://doi.org/10.1093/cercor/bhl054.

Clarke, A. M., Öğmen, H., & Herzog, M. H. (2016). A computational model for reference-frame synthesis with applications to motion perception. *Vision Research, 126*, 242–253. https://doi.org/10.1016/j.visres.2015.08.018.

Dakin, S. C., & Herbert, A. M. (1998). The spatial region of integration for visual symmetry detection. *Proceedings. Biological Sciences / The Royal Society, 265*(1397), 659–664. https://doi.org/10.1098/rspb.1998.0344.

Dakin, S. C., & Watt, R. J. (1994). Detection of bilateral symmetry using spatial filters. *Spatial Vision, 8*(4), 393–413.

Dakin, S. C., & Hess, R. F. (1997). The spatial mechanisms mediating symmetry perception. *Vision Research, 37*(20), 2915–2930. https://doi.org/10.1016/S0042-6989(97)00031-X.

Delius, J. D., & Nowak, B. (1982). Visual symmetry recognition by pigeons. *Psychological Research Psychologische Forschung, 44*(3), 199–212. https://doi.org/10.1007/BF00308420.

Delorme, A., & Makeig, S. (2004). EEGLAB: an open source toolbox for analysis of single-trial EEG dynamics. *Journal of Neuroscience Methods, 13*, 9–21. https://doi.org/10.1016/j.jneumeth.2003.10.009.

Feldman, J. (2007). Formation of visual "objects" in the early computation of spatial relations. *Perception & Psychophysics, 69*(5), 816–827. https://doi.org/10.3758/BF03193781.

Garner, W. R. (1974). The Processing of Information and Structure. *Earlbaum.*

Grammer, K., Fink, B., Møller, A. P., & Thornhill, R. (2003). Darwinian aesthetics: Sexual selection and the biology of beauty. *Biological Reviews of the Cambridge Philosophical Society, 78*(3), 385–407. https://doi.org/10.1017/S1464793102006085.

Heil, M. (2002). The functional significance of ERP effects during mental rotation. *Psychophysiology, 39*(5), 535–545. https://doi.org/10.1017/S0048577202020449.

Höfel, L., & Jacobsen, T. (2007). Electrophysiological indices of processing aesthetics: Spontaneous or intentional processes? *International Journal of Psychophysiology, 65*(1), 20–31. https://doi.org/10.1016/j.ijpsycho.2007.02.007.

Jenkins, B. (1983). Component processes in the perception of bilaterally symmetric dot textures. *Perception & Psychophysics, 34*(5), 433–440. https://doi.org/10.3758/BF03203058.

Julész, B. (1981). Figure and ground perception in briefly presented isodipole textures. In M. Kubovy, & J. R. Pomerantz (Eds.), *Perceptual organization* (pp. 27–54). Hillsdale, NJ: Erlbaum.

Keefe, B. D., Gouws, A. D., Sheldon, A. A., Vernon, R. J. W., Lawrence, S. J. D., McKeefry, D. J., … Morland, A. B. (2018). Emergence of symmetry selectivity in the visual areas of the human brain: fMRI responses to symmetry presented in both frontoparallel and slanted planes. *Human Brain Mapping, 39*(10), 3813–3826. https://doi.org/10.1002/hbm.v39.1010.1002/hbm.24211.

Kohler, P. J., Clarke, A., Yakovleva, A., Liu, Y., & Norcia, A. M. (2016). Representation of Maximally Regular Textures in Human Visual Cortex. *Journal of Neuroscience, 36*(3), 714–729. https://doi.org/10.1523/JNEUROSCI.2962-15.2016.

Koivisto, M., & Revonsuo, A. (2003). An ERP study of change detection, change blindness, and visual awareness. *Psychophysiology, 40*(3), 423–429. https://doi.org/10.1111/psyp.2003.40.issue-310.1111/1469-8986.00044.

Kourtzi, Z., & Kanwisher, N. (2001). Representation of perceived object shape by the human lateral occipital complex. *Science, 293*(5534), 1506–1509. https://doi.org/10.1126/science.1061133.

Kuai, S. G., Li, W., Yu, C., & Kourtzi, Z. (2017). Contour Integration over Time: Psychophysical and fMRI Evidence. *Cerebral Cortex, 27*(5), 3042–3051. https://doi.org/10.1093/cercor/bhw147.

Lauffs, M. M., Choung, O. H., Öğmen, H., Herzog, M. H., & Kerzel, D. (2019). Reference-frames in vision: Contributions of attentional tracking to nonretinotopic perception in the Ternus-Pikler display. *Journal of Vision, 19*(12), 1–15. https://doi.org/10.1167/19.12.7.

Locher, P. J., & Wagemans, J. (1993). Effects of element type and spatial grouping on symmetry detection. *Perception, 22*(5), 565–587.

Machilsen, B., Pauwels, M., & Wagemans, J. (2009). The role of vertical mirror symmetry in visual shape detection. *Journal of Vision, 9*(12), 1–11. https://doi.org/10.1167/9.12.11.Introduction.

Makin, A. D. J., Rampone, G., & Bertamini, M. (2015). Conditions for view invariance in the neural response to visual symmetry. *Psychophysiology, 52*(4), 532–543. https://doi.org/10.1111/psyp.12365.

Makin, A. D. J., Rampone, G., Morris, A., & Bertamini, M. (2019). The formation of symmetrical gestalts is task-independent, but can be enhanced by active regularity discrimination. *Journal of Cognitive Neuroscience, 32*(2), 353–366. https://doi.org/10.1162/jocn_a_01485.

Makin, A. D. J., Rampone, G., Pecchinenda, A., & Bertamini, M. (2013). Electrophysiological responses to visuospatial regularity. *Psychophysiology, 50*(10), n/a-n/a. https://doi.org/10.1111/psyp.12082.

Makin, A. D. J., Wilton, M., Pecchinenda, A., & Bertamini, M. (2012). Symmetry perception and affective responses : A combined EEG / EMG study. *Neuropsychologia, 50*(14), 3250–3261. https://doi.org/10.1016/j.neuropsychologia.2012.10.003.

Makin, A. D. J., Wright, D., Rampone, G., Palumbo, L., Guest, M., Sheehan, R., … Bertamini, M. (2016). An electrophysiological index of perceptual goodness. *Cerebral Cortex, 26*(12), 4416–4434. https://doi.org/10.1093/cercor/bhw255.

Marković, S., & Gvozdenovi, V. (2001). Symmetry, complexity and perceptual economy: Effects of minimum and maximum simplicity conditions. *Visual Cognition, 8*(3-5), 305–327. https://doi.org/10.1080/13506280143000025.

Martinovic, J., Jennings, B. J., Makin, A. D. J., Bertamini, M., & Angelescu, I. (2018). Symmetry perception for patterns defined by color and luminance. *Journal of Vision, 18*(8), 4. https://doi.org/10.1167/18.8.4.

Michotte, A., Thines, G., & Crabbé, G. (1964). Les complements amodaux des structures perceptives (Amodal completion of perceptual structures). Studia Psychologica. Publications Universitaires de Louvain.[GV].

Mojica, A. J., & Peterson, M. A. (2014). Display-wide influences on figure-ground perception: The case of symmetry. *Attention, Perception, and Psychophysics., 76*(4), 1069–1084. https://doi.org/10.3758/s13414-014-0646-y.

Niedeggen, M., Wichmann, P., & Stoerig, P. (2001). Change blindness and time to consciousness. *European Journal of Neuroscience, 14*(10), 1719–1726. https://doi.org/10.1046/j.0953-816x.2001.01785.x.

Niimi, R., Watanabe, K., & Yokosawa, K. (2005). The role of visible persistence for perception of visual bilateral symmetry. *Japanese Psychological Research, 47*(4), 262–270. https://doi.org/10.1111/j.1468-5884.2005.00295.x.

Niimi, R., Watanabe, K., & Yokosawa, K. (2008). The dynamic-stimulus advantage of visual symmetry perception. *Psychological Research Psychologische Forschung, 72*(5), 567–579. https://doi.org/10.1007/s00426-008-0133-y.

Noory, B., Herzog, M. H., & Ogmen, H. (2015). Retinotopy of visual masking and non-retinotopic perception during masking. *Attention, Perception, and Psychophysics, 77*(4), 1263–1284. https://doi.org/10.3758/s13414-015-0844-2.

Norcia, A. M., Candy, T. R., Pettet, M. W., Vildavski, V. Y., & Tyler, C. W. (2002). Temporal dynamics of the human response to symmetry. *Journal of Vision, 2*(2), 1. https://doi.org/10.1167/2.2.1.

Ogmen, H., Aydin, M., & Herzog, M. (2010). Differential perceived speeds explain the apparent compression in slit viewing, 197 197 *Journal of Vision, 7*(9). https://doi.org/10.1167/7.9.197.

Öğmen, H., & Herzog, M. H. (2016). A new conceptualization of human visual sensory-memory. *Frontiers in Psychology, 7*(JUN), 1–15. https://doi.org/10.3389/fpsyg.2016.00830.

Orlov, T., & Zohary, E. (2018). Object Representations in Human Visual Cortex Formed Through Temporal Integration of Dynamic Partial Shape Views. *The Journal of Neuroscience, 38*(3), 659–678. https://doi.org/10.1523/JNEUROSCI.1318-17.2017.

Osorio, D. (1996). Symmetry Detection by Categorization of Spatial Phase, a Model. *Proceedings of the Royal Society B: Biological Sciences, 263*(1366), 105–110. https://doi.org/10.1098/rspb.1996.0017.

Palmer, E. M., Kellman, P. J., & Shipley, T. F. (2006). A theory of dynamic occluded and illusory object perception. *Journal of Experimental Psychology: General, 135*(4), 513–541. https://doi.org/10.1037/0096-3445.135.4.513.

Palumbo, L., Bertamini, M., & Makin, A. (2015). Scaling of the extrastriate neural response to symmetry. *Vision Research, 117*, 1–8. https://doi.org/10.1016/j.visres.2015.10.002.

Peirce, J. W. (2007). PsychoPy - Psychophysics software in Python. *Journal of Neuroscience Methods, 162*(1–2), 8–13. https://doi.org/10.1016/j.jneumeth.2006.11.017.

Poirier, F. J. A. M., & Wilson, H. R. (2010). A biologically plausible model of human shape symmetry perception. *Journal of Vision, 10*(1), 1–16. https://doi.org/10.1167/10.1.9.

Quan, C., Li, C., Xue, J., Yue, J., Zhang, C., & Hamm, J. (2017). Mirror-normal difference in the late phase of mental rotation: An ERP study. *PLoS One, 12*(9), e0184963. https://doi.org/10.1371/journal.pone.0184963.

Rampone, G., & Makin, A. D. J. (2020). Electrophysiological responses to regularity show specificity to global form: The case of Glass patterns. *European Journal of Neuroscience, 2019*, 1–15. https://doi.org/10.1111/ejn.14709.

Rampone, G., Makin, A. D. J., Tatlidil, S., & Bertamini, M. (2019). Representation of symmetry in the extrastriate visual cortex from temporal integration of parts: An EEG/ERP study. *NeuroImage, 193*, 214–230. https://doi.org/10.1016/j.neuroimage.2019.03.007.

Reichert, C., Fendrich, R., Bernarding, J., Tempelmann, C., Hinrichs, H., & Rieger, J. W. (2014). Online tracking of the contents of conscious perception using real-time fMRI. *Frontiers in Neuroscience*. https://doi.org/10.3389/fnins.2014.00116.

Sasaki, Y., Vanduffel, W., Knutsen, T., Tyler, C., & Tootell, R. (2005). Symmetry activates extrastriate visual cortex in human and nonhuman primates. *Proceedings of the National Academy of Sciences of the United States of America, 102*(8), 3159–3163. https://doi.org/10.1073/pnas.0500319102.

Scharnowski, F., Hermens, F., & Herzog, M. H. (2007). Bloch ' s law and the dynamics of feature fusion. *Vision Research, 47*(18), 2444–2452. https://doi.org/10.1016/j.visres.2007.05.004.

Sharman, R. J., & Gheorghiu, E. (2017). The role of motion and number of element locations in mirror symmetry perception. *Scientific Reports, 7*(March), 45679. https://doi.org/10.1038/srep45679.

Sharman, R., & Gheorghiu, E. (2018). Spatiotemporal and luminance contrast properties of symmetry perception. *Symmetry, 10*(6), 220. https://doi.org/10.3390/sym10060220.

Sharman, R. J., & Gheorghiu, E. (2019). Speed tuning properties of mirror symmetry detection mechanisms. *Scientific Reports, 9*(1), 3431. https://doi.org/10.1038/s41598-019-39064-x.

Thielen, J., Bosch, S. E., van Leeuwen, T. M., van Gerven, M. A. J., & van Lier, R. (2019). Neuroimaging Findings on Amodal Completion: A Review. . *I-Perception, 10*(2). https://doi.org/10.1177/2041669519840047.

Treder, M. S., & van der Helm, P. A. (2007). Symmetry versus repetition in cyclopean vision: A microgenetic analysis. *Vision Research, 47*(23), 2956–2967. https://doi.org/10.1016/j.visres.2007.07.018.

Tyler, C. (1995). Empirical aspects of symmetry perception. *Spatial Vision*.

Tyler, C. W., Baseler, H. A., Kontsevich, L. L., Likova, L. T., Wade, A. R., & Wandell, B. A. (2005). Predominantly extra-retinotopic cortical response to pattern symmetry. *NeuroImage, 24*(2), 306–314. https://doi.org/10.1016/j.neuroimage.2004.09.018.

van der Helm, P. A., & Leeuwenberg, E. L. J. (1996). Goodness of visual regularities: A nontransformational approach. *Psychological Review, 103*(3), 429–456. https://doi.org/10.1037/0033-295X.103.3.429.

Van Meel, C., Baeck, A., Gillebert, C. R., Wagemans, J., & Op de Beeck, H. P. (2019). The representation of symmetry in multi-voxel response patterns and functional connectivity throughout the ventral visual stream. *NeuroImage, 191*(February), 216–224. https://doi.org/10.1016/j.neuroimage.2019.02.030.

Wagemans, J., Van Gool, L., & Dydewalle, G. (1991). Detection of symmetry in tachistoscopically presented dot patterns: Effects of multiple axes and skewing. *Perception & Psychophysics, 50*(5), 413–427. https://doi.org/10.3758/BF03205058.

Wagemans, J., Van Gool, L., Swinnen, V. V., & Van Horebeek, J. (1993). Higher-order structure in regularity detection. *Vision Research, 33*(8), 1067–1088. https://doi.org/10.1016/0042-6989(93)90241-N.

Wenderoth, P. (1994). The salience of vertical symmetry. *Perception, 23*(2), 221–236. https://doi.org/10.1068/p230221.

Wright, D., Makin, A. D. J., & Bertamini, M. (2017). Electrophysiological responses to symmetry presented in the left or in the right visual hemifield. *Cortex, 86*, 93–108. https://doi.org/10.1016/j.cortex.2016.11.001.

Wright, D., Mitchell, C., Dering, B. R., & Gheorghiu, E. (2018). Luminance-polarity distribution across the symmetry axis affects the electrophysiological response to symmetry. *NeuroImage, 173*, 484–497. https://doi.org/10.1016/j.neuroimage.2018.02.008.

Yin, C., Shimojo, S., Moore, C., & Engel, S. A. (2002). Dynamic Shape Integration in Extrastriate Cortex. *Current Biology, 12*(16), 1379–1385. https://doi.org/10.1016/S0960-9822(02)01071-0.

Zhu, T. (2014). Neural processes in symmetry perception: A parallel spatio-temporal model. *Biological Cybernetics, 108*(2), 121–131. https://doi.org/10.1007/s00422-013-0578-y.